Quantitative evaluation of human and climate forcing on erosion in the alpine Critical Zone over the last 2000 years

William Rapuc, Julien Bouchez, Pierre Sabatier, Kim Genuite, Jérôme Poulenard, Jérôme Gaillardet, Fabien Arnaud

Quantitative evaluation of human and climate forcing on erosion in the Alpine Critical Zone over the last 2000 years.

William Rapuc[1], Julien Bouchez[2], Pierre Sabatier[1], Kim Genuite[1,3], Jérôme Poulenard[1], Jérôme Gaillardet[2,4] and Fabien Arnaud[1]

(1) Univ. Grenoble Alpes, Univ. Savoie Mont Blanc, CNRS, EDYTEM, 73000 Chambéry, France

(2) Université de Paris, Institut de physique du globe de Paris, CNRS, F-75005 Paris, France

(3) UMR 6266 IDEES, University of Rouen Normandy, CNRS, 76130 Mont St-Aignan CEDEX, France

(4) Institut Universitaire de France

Corresponding Author:

William Rapuc

UMR CNRS 5204 Environnements, Dynamiques et Territoires de la Montagne (EDYTEM)

Université Savoie Mont Blanc, Campus scientifique,

73376 Le Bourget du Lac cedex, France

william.rapuc@univ-smb.fr

Abstract

Soil erosion is one of the main environmental threats affecting the Critical Zone (CZ) and thus ecosystem services and human societies. Through time, physical erosion is linked to both climate

variations and the landscape evolution under long-term human pressures. In mountainous areas where erosion is highest a combination of large spatial and temporal approaches allows to assess the effect of these forcing factors on erosion rates. Here, we apply a retrospective approach based on lake sediments to reconstruct the long-term evolution of erosion in alpine landscapes. Lake Iseo in the Italian Alps acts as a natural sink for all the erosion products from a large catchment (1777 km^2). This catchment is representative of the southern Italian Alps, where Holocene human activity and climate fluctuations are well known. The approach combines a source-to-sink method, using isotopic geochemistry (εNd, $^{87}Sr/^{86}Sr$) associated to a multiproxy study of a lacustrine sediment section covering the last 2000 years. The applied method allows us to disentangle the role of climate and land use as erosion forcing factors through their differential impact on the various rock types present in the catchment. Indeed, the high-altitude part of the Iseo catchment, where glacier advances and retreats drive the erosion, presents isotopic signature different from those of the sedimentary rocks located in the lower part of the catchment, where both human activities and precipitations impacted erosion through time. A chronicle of glacial erosion over the last 2000 years was produced. Once the climatic trend was highlighted, the signal of erosion of sedimentary rocks was investigated to understand the influence of humans. From the Roman Period to the Industrial Age several periods of deforestation and increased human pressure were documented. The past sediment yield inferred for sedimentary rocks exhibits the highest values (> 80 $t.km^{-2}.yr^{-1}$) at periods of intense human practices. Hence, since the late Roman Period, human activities seem to be the dominant forcing factor of the physical erosion in mountainous environment of northern Italy. This study presents the first reconstruction through time of sediment yield derived from lake sediments associated with sediment sources identification and quantitative evaluation of the CZ erosion drivers.

Keywords

Erosion, Human impact, Lake sediments, Source to sink method, isotopic mixing model

1. Introduction

Erosion is a geological process that, on long timescales, impacts the Earth's topography, tectonics and climate (e.g. Gayer et al., 2019 and references therein). Currently, erosion is also the main process leading to the deterioration of the Critical Zone (CZ), defined as the thin active layer at the Earth's terrestrial surface, which host life forms. Among other impacts, by destroying soils, erosion alters food production, drinking water quality, ecosystems services, biodiversity, and soil carbon stocks (e.g. Bosco et al., 2008; Panagos et al., 2015). Erosion also directly affects human societies (Montgomery, 2012), especially in mountainous environments (Bosco et al., 2008) and has thus become a scientific subject of prime importance worldwide (Borrelli et al., 2020; FAO, 2015; Panagos et al., 2015; Rusco et al., 2008). Increasing concern about these deleterious effects has led Europe and the United Nations to rank soil erosion as one of the main threats to mankind, and to call for quantitative evaluation of soil loss over large spatial and long temporal scales (e.g. Panagos et al., 2015 and references therein). The objective of these evaluations is to better assess the relative effects of the main factors controlling erosion. In particular, climate (for example through the precipitation regimes or glaciers advances and retreats) and human activities (through land-use and vegetation cover management) have been identified as major controls on long-term changes in erosion rates (e.g. Panagos et al., 2015).

Besides the use of modelling approaches (e.g. Angima et al., 2003; Borrelli et al., 2020; Millward and Mersey, 1999; Panagos et al., 2015; Renard et al., 1991), this knowledge gap can be filled through the acquisition of empirical constraints provided by the study of lake sediment archives, in particular with the aim of evaluating erosion rates over the centennial to millennial time scales over which climatic and human forcing are the most likely drivers of erosion (e.g. Arnaud et al., 2016). Although regional syntheses of erosion rates over these time scales exist, in particular for the European Alps (e.g. Hinderer et al., 2013 and references therein), only a few studies have produced a quantitative assessment of erosion rates through time (e.g. Bajard et al., 2020), but none on the quantitative impact of the various factors. The "source-to-sink" approach (e.g. Collins and Walling, 2002) offers the

69 possibility to track the sources of sediment inputs (sub-catchments and/or rock types) to a sink (e.g.,
70 a lake) through time, making it in turn possible to disentangle the relative impacts of climate and
71 human activities upon erosion rates, provided that each sediment source is sensitive to a given type of
72 forcing.

73 For this study, we selected Lake Iseo, located in the Italian Alps, at the downstream end of the Val
74 Camonica valley, an area where human activities since the beginning of the Neolithic period are well
75 documented (e.g. Pini et al., 2016 and references therein). Lake Iseo drains a large catchment that can
76 be split into three main sediment source areas, distinguishable through the means of geochemical
77 tools, and coinciding with different relative roles of climatic and human forcings on erosion over the
78 centennial to millennial scales:

79 (i) The northernmost, high-altitude part of the catchment underlain by calco-alkaline rock
80 series and where numerous glaciers have shaped the landscape (Scotti et al., 2013);
81 (ii) The mid- to high-altitude part of the catchment underlain by metamorphic Variscan
82 basement rocks where both glaciers and human activities have impacted erosion (Pini et
83 al., 2016; Scotti et al., 2013)
84 (iii) The southernmost, low- to mid-altitude part of the catchment underlain by Permian to
85 Cretaceous sedimentary cover, and the locus of most human activities in the Val Camonica
86 since the beginning of the late Holocene (Pini et al., 2016 and references therein).

87 To quantify the evolution of erosion in the catchment of Lake Iseo over the late Holocene, we selected
88 a sediment sequence retrieved in the deep depositional basin of the lake, where most of the fine-
89 grained sediment inputs from the catchment have been captured. River samples were also collected
90 from all the sub-catchments directly contributing to Lake Iseo. Neodymium (Nd) and Strontium (Sr)
91 isotopic compositions and concentrations of river and lake sediments were used to constrain the
92 results of a mixing model (for discussion of the model please refer to sub-section 4.3). Results from the
93 model yielded quantitative contributions of each sediment source, allowing us to disentangle the

effects of climate fluctuations and human activities on erosion in the Iseo catchment from the Roman Period to the present day.

2. Study sites

Lake Iseo (45°44.205'N; 10°4.340'E) lies in the Italian Alps, at the southern end of the Val Camonica valley at an altitude of 185 m a.s.l (above sea level). The lake is 25-km long and has a surface area of 60.9 km^2.

Lake Iseo is fed water and sediment by the Oglio River, which originates in the Adamello Massif, and is the main lake tributary and unique outlet (**Fig. 1**). Upstream from Lake Iseo, the Oglio River drains a large catchment of 1777 km^2 with a maximum elevation of 3539 m a.s.l in the Adamello Massif and a mean altitude of 1400 m a.s.l (Garibaldi et al., 1999). The Oglio catchment is limited to the North and East by the Insubric line, one of the main lineaments of the European Alpine (Mittempergher et al., 2021), separating the Austroalpine domain (N) from the southern Alps (S). Rocks of high alpine metamorphic grade from the Austroalpine unit exist at the extreme northern limit of the catchment but constitute very small areas (Chiesa et al., 2011; Gosso et al., 2012).

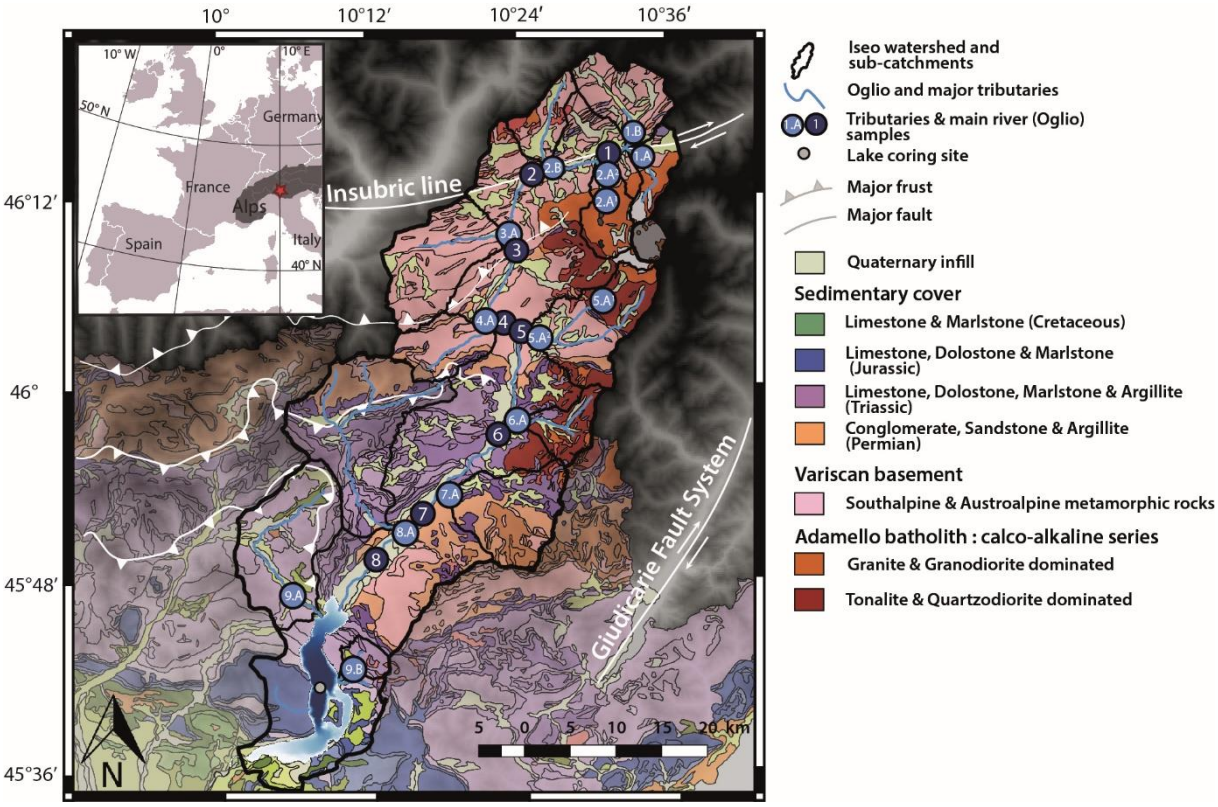

Figure 1 – Geological map of the study area, superimposed on a shaded relief map, and location of sampling sites. The geological information is modified from the geological map of Lombardy (CARG project; https://www.cartografia.servizirl.it/cargviewer/). The tributaries (blue) and sub-catchments (boundaries in black) of the Oglio River and the SEB18 lake sediment coring site are also shown (grey circle). Lake Iseo bathymetry is modified from Pilotti et al. (2013) and is available at https://hydraulics.unibs.it/hydraulics/attivita-scientifica/laghi_pvbs/lake-iseo-data-set/.

The faulted Variscan basement of the southern Alps is made of low- to high-grade metamorphic rocks (pelites, schists, amphibolites, gneiss) visible in the North and West part of the Upper Oglio catchment. To the South, the catchment is underlain by the sedimentary cover of the southern Alps, mainly composed of Triassic, Jurassic, and Cretaceous marlstones, limestones, and dolostones, associated with outcrops of Permian sandstones (Bini et al., 2012).

The NE part of the catchment area is underlain by the famous Adamello batholith which is a plutonic series of calco-alkaline rocks of Cenozoic age (30 to 40 Ma) that intruded the old southern Alps Variscan basement (Mittempergher et al., 2021). The Adamello massif is mainly composed of felsic plutonic rocks such as tonalites, granites, granodiorites, and quartzodiorites, with some minor outcrops of mafic

to ultramafic rocks (Brack et al., 2008). Glaciers and rock glaciers are particularly numerous in this part of the catchment (Scotti et al., 2013) and are suspected to have strongly impacted erosion in the area.

In terms of human occupation, the southernmost area, closest to the lake, is located at low to mid altitude, and is where human activities are currently concentrated (**Fig. 2**). Archaeological and palynological studies also locate the main human settlements and agrarian activities within this area since the Neolithic (e.g. Marziani and Citterio, 1999; Pini, 2002; Pini et al., 2016). Human activities in the rest of the catchment area are sparse, restricted to herd grazing and only minor urban areas, both for modern times (**Fig. 2**) and in the recent past (Pini et al., 2016).

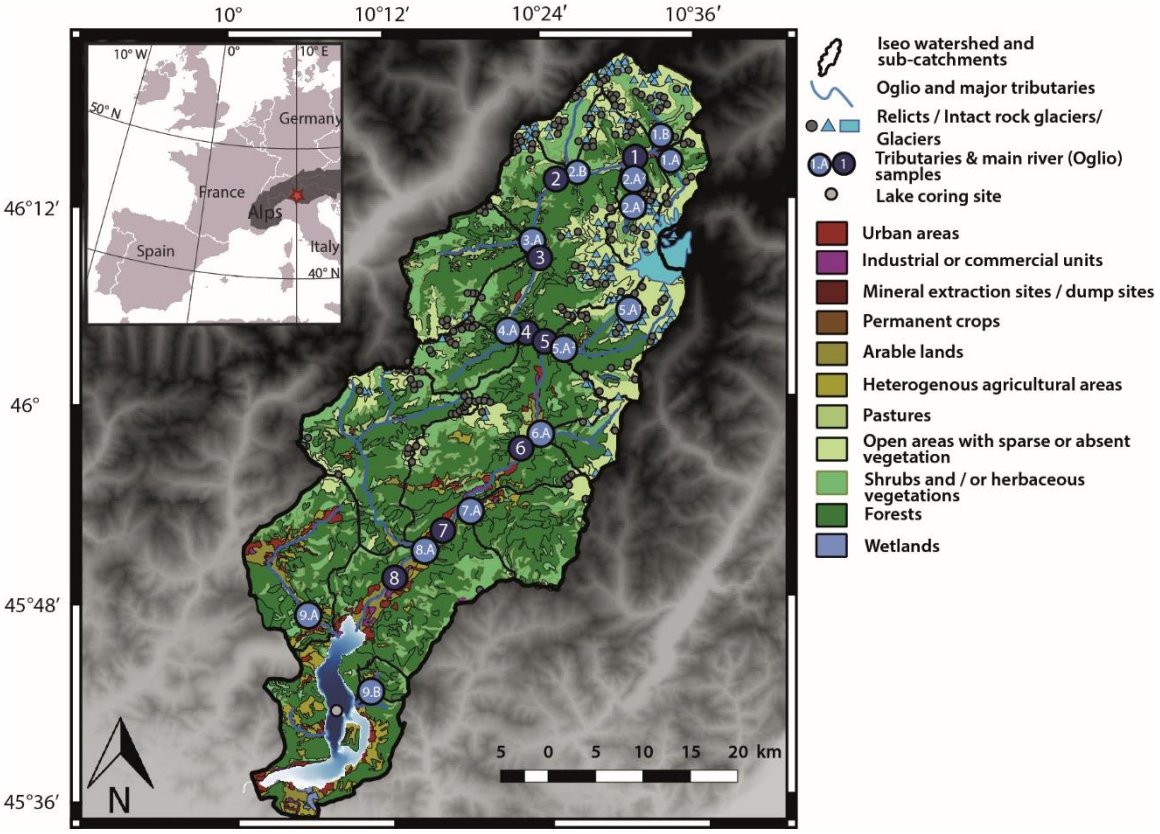

Figure 2 – Land-use map of the study area, superimposed on a shaded relief map, and location of sampling sites. Land use information is derived from the CORINE land cover map for Lombardia, available here: http://www.geoportale.regione.lombardia.it/. Locations of glaciers, relicts, and intact rock glaciers are derived from Scotti et al. (2013).

3. Materials and Methods

3.1. Lake sediment

In October 2018, a 15.5-m-long sediment sequence coded "SEB18" (45°43.536'N; 10°3.888'E) was retrieved from the deep basin of Lake Iseo, at 251 m below the lake surface (b.l.s). This site was selected as it is supposed (i) to be less influenced by event sedimentation (Bini et al., 2007) and (ii) to have collected the sediment input from the Oglio River in a continuous way. For this survey, two UWITEC 90-mm diameter piston corers (Uwitec, Mondsee, Austria) were used, operated from an UWITEC platform (EDYTEM/LSCE/C2FN). Most of the sections were split, photographed at high-resolution (20 pixels.mm^{-1}), described and logged in detail. The identification of specific layers on the overlapping sections allowed the creation of the composite sediment sequence.

Thirty 1 cm-long sediment samples were collected from the background sedimentation (**supplementary Table S1 & S2**) using graduated syringes for geochemical analyses (sections 3.4 and 3.5). Due to the presence of multiple event-specific sediment layers, a continuous sampling step was impossible to apply. Sediment dry bulk density (DBD) was measured using sediment samples of an invariant 5 mL volume.

Loss-on-ignition measurements were conducted on all the sediment samples following the method of Heiri et al. (2001). The proportion of detrital silicates in the sediment samples was evaluated from values of non-carbonate residue (NCIR) that is the sediment remaining after the last ignition step (950° for 2h; Bajard et al., 2016).

To produce a precise age-depth model for the sediment sequence, we combined varve counting, short-lived radionuclides (^{210}Pb, ^{137}Cs, ^{241}Am), and ^{14}C. Varves were counted over the first 37 cm of the core, then 38 samples were collected over the first 48.1 cm of the sequence to measure short-lived radionuclide activities at the Laboratoire Souterrain de Modane using the well-type germanium detectors (Reyss et al., 1995). Short-lived radionuclide chronology was carried out using the R code

160 package “serac” (Bruel and Sabatier, 2020). Thirteen samples of vegetal macro-organic remains were
161 used to perform ^{14}C measurements at the LMC14 laboratory (CNRS) using AMS. Dates were calibrated
162 at 2 sigma using the Intcal20 calibration curve (Reimer et al., 2020), and the age-depth model was
163 performed using R code packages “clam” (Blaauw, 2010) and “bacon” (Blaauw et al., 2021) in R
164 software.

165 3.2. River sediment samples

166 To characterize the source of sediments accumulated in Lake Iseo deep basin, 14 river sediment
167 samples were collected in May 2018 from flood deposits in all sub-catchments directly contributing to
168 the Oglio River, close to the confluence with the main river (**Fig. 1**; **Table S3**). Eight samples were also
169 collected from flood deposits in the Oglio main valley at several hundred meters downstream of each
170 confluence to test for the mixing between sub-catchment and main river sediments (**Fig. 1**; **Table S3**).
171 Sub-catchments covered by this sampling set represent 52 % of the Iseo catchment total area. Samples
172 were collected manually, an aliquot of each sample was sieved, and only the fraction finer than 63 µm
173 was saved for later analysis, to account for the fact that the sedimentation in the studied lake sediment
174 core is mostly of silty to clayey nature.

175 3.3. Sample preparation

176 Even in carbonate-dominated terrains, soil physical erosion occurs mostly through the removal of
177 silicate phases, as carbonate minerals tend to be removed from soils through chemical dissolution. For
178 this reason, our analysis focuses on siliciclastic material, and we removed the carbonate component
179 of the lake and river sediments before geochemical analyses. Although the authigenic carbonate
180 production is poorly preserved in the deep basin of peri-Alpine lakes (Ramisch et al., 1999), this
181 procedure also ensures that authigenic lake carbonates do not affect our interpretation. To that effect,
182 after crushing in an agate mortar and drying at 60°C for 72 h in a laboratory oven, river and lake
183 sediment samples were decarbonated by two successive 5 mL HCl 0.5N leaching steps to remove
184 authigenic and detrital carbonate (**supplementary S4**). Major and trace elements of supernatants from

each leaching step were measured by Q-ICP-MS (section 3.2) to evaluate the amount of calcium (Ca) and Sr lost. As discussed below, this leaching procedure did not lead to complete removal of the carbonate component from the river sediment samples, which might be due to the presence of dolomite in the sediment.

A series of river sediment samples was kept unleached and measured as bulk powder for isotope and major and trace element concentration measurements. All samples (bulk or residue from the leaching steps), then underwent a digestion using concentrated acid mixtures of HF, HNO_3, and HCl.

3.4. Major and trace elements

Major and trace element concentrations were measured using an Agilent 7900 quadrupole ICP-MS (Q-ICP-MS) at the High-Resolution Analytical Platform (PARI) of the Institut de physique du globe de Paris (IPGP). Liquid samples were sprayed through a micro-nebulizer in a Scott spray chamber prior to ionization. Magnesium (Mg), calcium (Ca), and iron (Fe) were measured using a collision-reaction cell with helium gas (5 $mL.min^{-1}$) to remove polyatomic interferences. Nd and Sr were measured without collision gas. Signal drift and matrix effects were corrected by injection of scandium, indium, and rhenium as internal standards after inline mixing with the samples. Two sets of multi-element calibration standards (one for major and one for trace elements) were analysed to compute the calibration curves that were used to convert measured counts to concentrations. The reported uncertainties were calculated using the algebraic propagation of blank subtraction and sample count standard deviations (n=3). The NIST®SRM®2709a reference material (San Joaquin soil) was processed as samples and analysed repeatedly during the sequences to evaluate the accuracy of the measurements. The detection limit was between 0.2 and 0.5 ppt depending on the element, and the internal errors were 5% on average. The weight loss during carbonate leaching of lake (and river in some cases) sediments was considered in the estimate of major and trace element concentrations of the residue, such that the reported concentrations relate to the mass of residue (that is, carbonate-

free, and referred to as “silicate” in the following) component of the sediment (**see supplementary S4**).

3.5. Isotopic composition

Isotope measurements were all performed at the PARI analytical platform of IPGP. After powder digestion, Sr and Nd were separated from the sample matrix by extraction chromatography. We used an Sr-SPEC resin (Eichrom) for Sr (Hajj et al., 2017) and a combination of TRU-spec and Ln-spec resins for Nd (Cogez et al., 2015).

Sr isotope ratios were measured by multi-collector inductively coupled plasma mass spectrometry (MC-ICPMS; Neptune, Thermo-Fisher Scientific) with an APEX-Q (ESI) desolvation system as a sample introduction system. Rubidium (Rb, that was observed in residual amounts in some samples, even after chromatographic purification) interference on mass 87 and krypton (Kr, present in the argon gas used to produce the plasma) interferences on masses 84 and 86 were corrected for using the ^{85}Rb and ^{83}Kr signals along with the Rb and Kr isotope ratios measured at the beginning of the sequence. Instrumental and natural mass fractionation on the ^{87}Sr/^{86}Sr ratio were corrected using an exponential law, the measured ^{88}Sr/^{86}Sr ratio and the “natural” abundance ^{88}Sr/^{86}Sr ratio assumed to be equal to 8.3752. Measurement accuracy was checked through repeated measurements of the NIST pure-Sr, isotope reference material SRM 987 (2 S.D of 2.9 x 10-5), and the NIST soil reference material SRM 2709a (^{87}Sr/^{86}Sr = 0.70823 ± 0.00002; comparing well with the value provided by Brazier et al., 2020 of 0.70814 ± 0.00002). Each sample was measured up to three times during a session. For samples measured three times, the 95% confidence interval was obtained from Student’s t-distribution and ranged from 3 x 10^{-6} to 8 x 10^{-3}. For other samples measured less than 3 times, the 2 S.D of 4.9 x 10^{-5} estimated from the repeated measurements of the reference material NIST SRM 2709a (processed through powder digestion and separation as for samples) was used as an estimate of the 95% confidence interval.

Nd isotope analyses were performed by MC-ICP-MS Neptune using N_2 addition and X-cones with an APEX-IR (ESI) desolvation system as the sample introduction system. Instrumental and natural mass fractionation on the $^{143}Nd/^{144}Nd$ ratio were corrected for using an exponential law, the measured $^{146}Nd/^{144}Nd$ ratio and its natural abundance ratio, taken as 0.7218. Accuracy was checked through repeated measurements of a NIST pure-Nd, isotope reference material ($^{143}Nd/^{144}Nd$ = 0.511418; Caro et al., 2006), with a measured 2 S.D of 2.7 x 10^{-6}, and the NIST soil reference material SRM2709a (0.512381 ± 0.000028). For convenience we report Nd isotope ratios as εNd values:

$$\varepsilon\mathrm{Nd} = \left(\frac{\left(^{143}\mathrm{Nd}/^{144}\mathrm{Nd}\right)_{samples}}{\left(^{143}\mathrm{Nd}/^{144}\mathrm{Nd}\right)_{CHUR}} - 1\right) \times 10\,000$$

with $\left(^{143}\mathrm{Nd}/^{144}\mathrm{Nd}\right)_{CHUR}$ (CHUR standing for "chondritic uniform reservoir") equal to 0.512638 (Jacobsen and Wasserburg, 1980). Each sample was measured twice during a session, and the 95% confidence interval of the measurement was estimated from the 2 S.D. at 0.4 εNd unit from repeated measurements of the NIST reference material SRM2709a at mass spectrometric signal levels similar to those of samples.

4. Results and interpretations

All the results of lake (sink) and river (source) sediment geochemistry, dating and sedimentology are presented in **Figs. 3 and 4** and in **supplementary Table S1, S2, S3 & S5**.

4.1. Lake sediments

In the SEB18 sediment section, background sedimentation accounts for 39 % of the total sediment accumulation and is composed mainly of grey clay, visually distinguishable from homogenite or turbidite-type graded layers interpreted as event layers. Over the 15.5 m of sediment, 146 event layers (≥ 1 mm) have been identified and represent 61 % of the sediment. The material making the background sedimentation of the lake Iseo deep basin mainly consists of detrital silicates. Indeed, most of the lake authigenic carbonate is dissolved within the water column whereas the organic matter

content is under 8 %, and detrital carbonates account for less than 18 %. NCIR mean value in the background sedimentation is 82.5 % and increase progressively towards the bottom of the sequence (**see supplementary S1**).

The age depth-model of the SEB18 sequence was constrained by a combination of short-lived radionuclides, varve counting, and ^{14}C ages, detailed information is presented **in supplementary S5**. To constrain the upper part (0 – 48 cm) of the sediment section, we used ^{137}Cs and ^{241}Am profiles, that present two peaks (16.7 – 19.7 and 42.5 – 43.5 cm) that are widely attributed to the 1986 CE Chernobyl accident (e.g., Appleby et al., 1991) and to the maximum nuclear weapon tests at 1963 CE (Appleby et al., 1991b). These peaks, in good agreement with the varve counting model and the ^{210}Pb excess profile ($^{210}Pb_{ex}$), are used as chronological markers to construct the age-depth model of the entire SEB18 sediment section. Thirteen samples of terrestrial macro-remains were analyzed to provide radiocarbon ages for the rest of the sediment section. Once calibrated, 4 of these 13 dates were not used because they presented ages older than the best-fit age-depth curve of the SEB18 sequence. The thickness of each event layer was subtracted from the SEB18 sediment sequence depth to create an event-free depth and to obtain the best age-depth model. The obtained SR was calculated from the event-free depth and is not influenced by the variation of the event layer occurrence (**Fig. 3**). To reduce the SR uncertainty linked to the first radiocarbon age, we decided to use only the uncertainty of the short-lived radionuclides and the other radiocarbon ages.

The SEB18 sequence covers the last 2000 yrs (21 – 2018 CE) with a continuous SR that varies between 5.1 and 2.1 $mm.yr^{-1}$, with a mean of 3.1 $mm.yr^{-1}$. Three periods of gradual increase of SR are identified in the sequence: (i) between 500 and 800 CE (SR max = 3.2 $mm.yr^{-1}$), (ii) between 1000 and 1400 CE (SR max = 3.06 $mm.yr^{-1}$) and (iii) from 1500 CE towards the top (SR max = 5 $mm.yr^{-1}$).

In the siliciclastic fraction of Iseo Lake sediments, the $^{87}Sr/^{86}Sr$ ratio ranges between 0.730 and 0.722 with a significant increase from 97 to 1033 CE followed by a decrease until 1265 CE, and then relatively high values with successive high and lows until the present day (**Fig. 3**). Values of εNd are relatively

281 invariant and range between -11.8 and -10.4 (**Fig. 3**), with only two notable excursions towards higher
282 values from 907 to 1185 CE and from 1551 to 1872 CE.

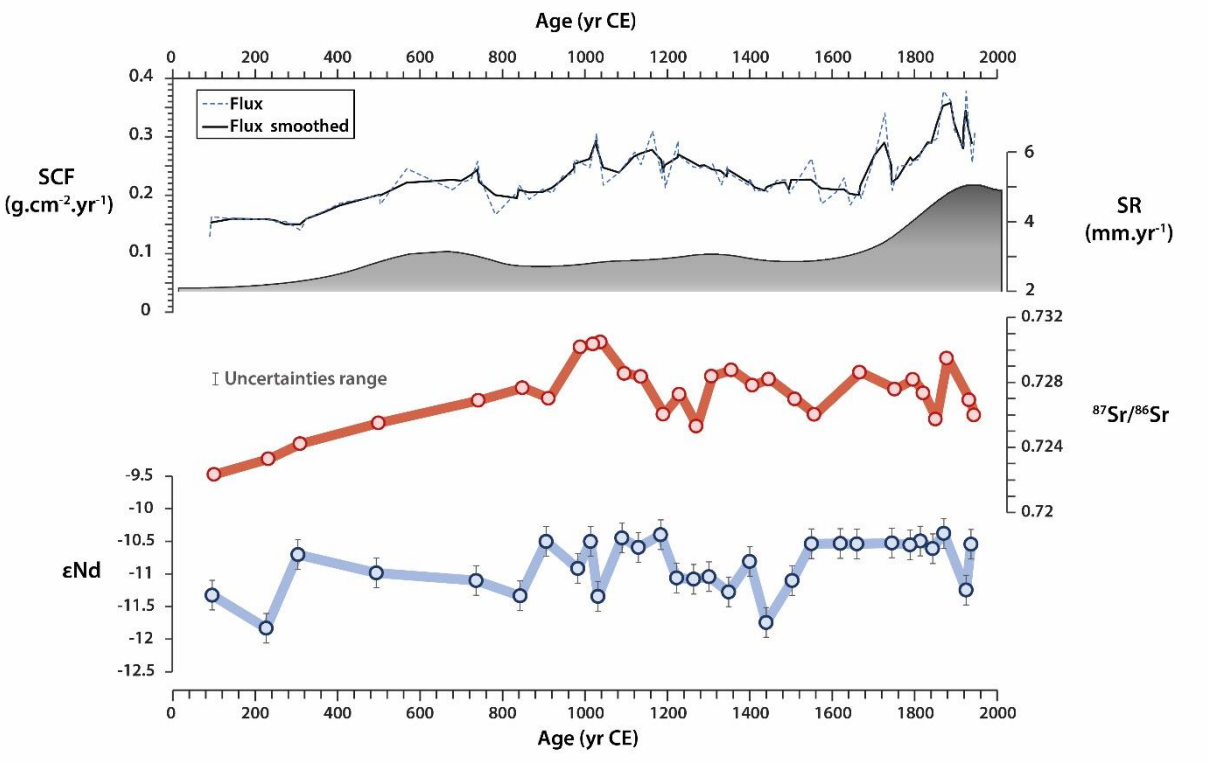

283

284 *Figure 3 – Silicate detrital flux (SCF, for siliciclastic flux), sedimentation rate (SR) and Sr and Nd isotope ratios of Lake Iseo over*
285 *the last 2000 years obtained from lake sediment SEB18 sediment sequence. The siliciclastic flux was obtained from loss on*
286 *ignition analyses, age-depth modelling and density measurements (**supplementary S1**). The sedimentation rate was obtained*
287 *from the age-depth model (**supplementary S5**). Error bars on the $^{87}Sr/^{86}Sr$ and εNd curves represent the 95% confidence*
288 *intervals corresponding to analytical uncertainty.*

289 ## 4.2. River samples

290 River sediments taken in Oglio sub-catchments are characterized by εNd values ranging from -5.5 to -
291 13.4 (**Fig. 4**). Sediment samples from the northern, high-altitude basins, thus reflective of the calco-
292 alkaline-type rock sources present the most radiogenic values: -5.5 to -6.3 for sub-catchments
293 essentially underlain of tonalites (6.A and 5.A1) and -8.4 to -9.7 for granite dominated sub-catchments.
294 Southern sub-catchments draining sedimentary rocks display εNd values ranging from -8.3 to -10.5,
295 while sub-catchments dominated by Variscan metamorphic rocks present the highest variability in εNd
296 values, from -10.1 to -13.4.

$^{87}Sr/^{86}Sr$ ratios for leached river sediment samples range from 0.708 to 0.726. Northern Oglio sub-catchments dominated by calco-alkaline series display low $^{87}Sr/^{86}Sr$ values, from 0.708 for tonalite-dominated catchments to 0.712 for granite-dominated catchments. Sub-catchments underlain mostly by Variscan metamorphic rocks are characterized by $^{87}Sr/^{86}Sr$ ratios ranging from 0.718 to 0.723. Southern sub-catchments draining sedimentary rocks present $^{87}Sr/^{86}Sr$ ratios from 0.725 to 0.726. At face value, none of the $^{87}Sr/^{86}Sr$ ratios from the sampled sub-catchments can explain the most radiogenic ratios observed in lake sediments (**Fig. 4**). Bulk values are presented in **Table S3 and Fig. S6.1** and display systematically lower $^{87}Sr/^{86}Sr$ values for sub-catchments where limestones and dolostones crop out.

Oglio River samples εNd values range between -7.5 and -11.8, whereas their $^{87}Sr/^{86}Sr$ ratios range from 0.716 to 0.721 (**Fig. 4**).

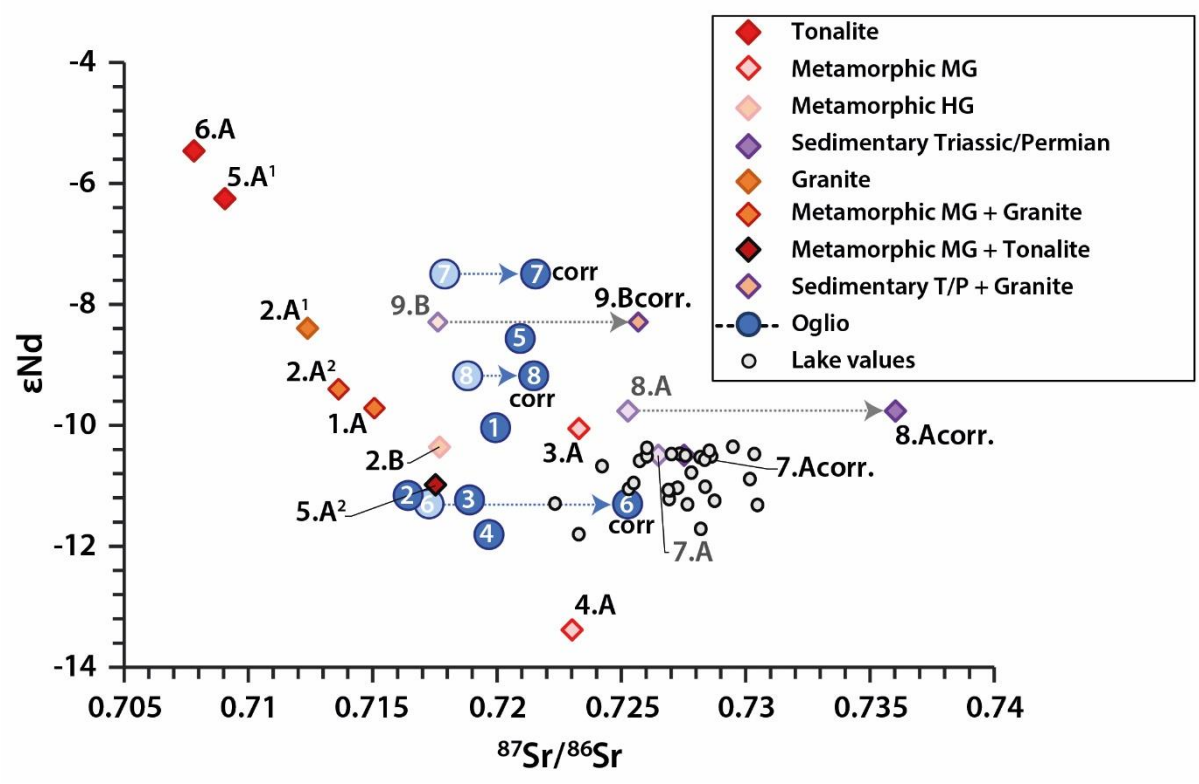

Figure 4 – Nd and Sr isotope composition of Lake Iseo siliciclastic sediment samples (small grey circles), and of river sediment samples from the Oglio sub-catchments upstream from Lake Iseo (diamonds) and from the Oglio main valley (large blue circles). Oglio sub-catchments symbols (diamonds) are coloured as a function of the dominant rock types underlying the catchment. Oglio main valley sediment samples (blue circles) are numbered as in Figs 2 and 3. Dotted arrows represent the

*correction from carbonate contribution performed for river samples originating from sub-catchments underlain by limestone, as constrained by mild acid leaching steps (section 3.1; **supplementary S4**).*

4.3. Interpreting Sr and Nd isotope ratios in term of sediment source fingerprinting

Two main assumptions are made here for the interpretation of the Sr and Nd isotope data from Lake Iseo and Oglio River in terms of the contribution of each rock source to the detrital sediment input to the lake:

- All the major sediment sources contributing to detrital inputs to the lake were sampled.
- The isotopic signatures of the various potential rock sources have remained constant over the period considered.

Because we removed the carbonate component of the lake and river sediments, the Sr-Nd isotope signatures of lake samples can be interpreted as a mixture of the identified silicate sources. In order to quantitatively deconvolve the contributions of the dominant rock sources through time, end members need to be identified, and their signatures need to be constrained. To that effect, we selected sediment samples from sub-catchments presenting a homogeneous lithology (**Fig. 5A**). Indeed, samples from the Oglio River and sub-catchments with heterogeneous lithology (**Fig. 1**) result from a mixture of several rock sources on their own, such that considering them would not provide independent constraints on the composition of the end members. River sediment samples for which only one out of the two isotope signatures was available were not considered either.

Out of the remaining 8 samples, three main sources can be identified and summarized into: i) calco-alkaline rocks ("A"), ii) metamorphic ("B") and iii) sedimentary ("C") rock sources.

Sub-catchments draining mainly rocks from the calco-alkaline rock series (6.A, $5.A^1$, $2.A^1$) were gathered into a single "calco-alkaline rocks" source. Minor marlstone and limestone outcrops are also present in these areas, especially in $2.A^1$ sub-catchment (**Fig. 1**) which may explain the lower εNd values measured for some sub-catchment samples compared to the values reported for the rocks

themselves (+3.8 to -4.9; Kagami et al., 1991). This end member is sourced from the high-altitude Adamello massif (**Fig. 1**). Several glaciers and rock glaciers are currently present in this area (Scotti et al., 2013). Sr-Nd isotope signatures of the sample 6.A (**Fig. 4**) were selected as a fingerprint of the contribution of the calco-alkaline rocks source, as this sample is the closest to the Adamello massif outcrops signature (Kagami et al., 1991).

Sub-catchments draining mostly metamorphic rocks were combined into the "metamorphic" source. We note that these catchments are also partially underlain by sedimentary rock outcrops and Quaternary deposits. Samples from this source (2.B, 3.A and 4.A) present contrasted Sr-Nd isotope signatures, linked to their heterogeneous composition (**Fig. 4**). The sub-catchment of sample 4.A presents the highest proportion of metamorphic rocks (**Fig. 1;** https://www.cartografia.servizirl.it/cargviewer/), which constitutes the only rock source that can explain the lowest εNd values observed in lake sediment samples (**Fig. 4**). As a consequence, the isotope signatures of sample 4.A are used as a fingerprint for the contribution of metamorphic rocks in the Lake Iseo catchment. Due to the significant heterogeneity of the metamorphic source, the fractional input from this end member to Lake Iseo sediments over time are discussed with great caution hereafter.

The remaining samples 7.A and 8.A originate from sub-catchments dominated by sedimentary rocks and were thus gathered into the "sedimentary rock" source. This source shows εNd values between -10.5 and -9.7, associated to the highest $^{87}Sr/^{86}Sr$ ratios (> 0.725). However, these $^{87}Sr/^{86}Sr$ values are not high enough to explain the highest $^{87}Sr/^{86}Sr$ ratios observed in lake sediment samples. This is because the sub-catchments dominated by sedimentary rocks are actually underlain by marlstones and limestones/dolostones. Although our decarbonation protocol has likely removed a large fraction of the carbonate component present in the river sediment, we expect that relatively refractory carbonate minerals such as dolomite remain in the "silicate" residue of the leaching procedure. As a consequence, this residue hosts a non-silicate component, most likely characterized by relatively low $^{87}Sr/^{86}Sr$ ratios (Faure et al., 1978), and the contribution of which needs to be corrected for. Details

about this correction are provided in **supplementary S6**. After correction, the Sr signature of river sediments from sub-catchments draining sedimentary rocks is sufficiently ^{87}Sr-enriched to explain the highest $^{87}Sr/^{86}Sr$ ratios observed in Lake Iseo sediments (**Fig. 4**). Areas corresponding to the "sedimentary rock" source are located at low to mid altitude, in the southern part of the Iseo catchment, and correspond to places of current intense human activities (**Fig. 2**). The Nd-Sr isotope signatures of sample 8.A were selected as a fingerprint of the "sedimentary rock" source as this sub-catchment presents the highest proportion of marlstone (**Fig. 1;** https://www.cartografia.servizirl.it/cargviewer/) and is the only one explaining the most radiogenic $^{87}Sr/^{86}Sr$ signature observed in lake samples.

The fractional contribution of each rock source can be estimated using a mixing model. The lake sediment Sr and Nd isotope compositions depend on (i) the Sr-Nd concentration and isotope signatures of each rock source, and (ii) the proportion of each contributing source in the mixture. This can be summarized by a system of 5 linear equations, expressed as follows:

$$[Sr]^M = [Sr]^A \times f_A + [Sr]^B \times f_B + [Sr]^C \times f_C \quad (1)$$

$$[Nd]^M = [Nd]^A \times f_A + [Nd]^B \times f_B + [Nd]^C \times f_C \quad (2)$$

$$f_A + f_B + f_C = 1 \quad (3)$$

$$\frac{^{87}Sr}{^{86}Sr}^M \times [Sr]^M = \frac{^{87}Sr}{^{86}Sr}^A \times [Sr]^A \times f_A + \frac{^{87}Sr}{^{86}Sr}^B \times [Sr]^B \times f_B + \frac{^{87}Sr}{^{86}Sr}^C \times [Sr]^C \times f_C \quad (4)$$

$$\varepsilon Nd^M \times [Nd]^M = \varepsilon Nd^A \times [Nd]^A \times f_A + \varepsilon Nd^B \times [Nd]^B \times f_B + \varepsilon Nd^C \times [Nd]^C \times f_C \quad (5)$$

with the superscript M standing for lake sediment ("mixture") values, and the superscripts A, B and C stand for the three rock sources values (calco-alkaline rocks, metamorphic, and sedimentary rocks, respectively); f_x represents the fractional contribution of each rock source.

Solving this equation system leads to estimates of the relative contributions of sources A, B and C. Analytical solutions for f_A, f_B and f_C were obtained from Maple software (**see supplementary S7**). A

Monte Carlo method was used to compute uncertainties on the fractional contributions. Random sampling within the analytical uncertainties of each parameter was executed using a Box–Muller transform (Box and Muller, 1958) for each of the 5000 iterations of the Monte Carlo procedure. From the simulated parameter distributions, D84, D16, median and standard deviation were obtained for each proportion f_x (**Table S8**). The "sedimentary rocks" source contributes on average to $79.6^{+4.8}_{-5.7}$ % of the total siliciclastic sedimentation in Lake Iseo deep basin, whereas the calco-alkaline rocks source is the smallest contributor with a mean contribution of $3.5^{+1.8}_{-1.5}$ % and the metamorphic source contribute to $16.7^{+6.1}_{-5.0}$ % on average (**Fig. 5B**). Through the last 2000 years, the "sedimentary rock" inputs to Lake Iseo remain predominant and increase progressively towards the Middle Ages and the Industrial Age.

Beyond accounting for analytical uncertainties, an additional sensitivity test was run to evaluate the impact of the Sr-Nd isotope signatures selected for each rock end member. "Geological" uncertainties of 0.005 on the $^{87}Sr/^{86}Sr$ ratio and of 0.8 epsilon-units on εNd, together with a 50 % relative uncertainty on Nd and Sr concentrations were attributed to each end member, and a Monte Carlo procedure was performed in the same manner as that laid out above (**Table S9** and **Fig. 5B**). Regardless of the exact composition of the three end members within the ranges given above, the "sedimentary rocks" source remains the predominant contributor to the continuous accumulation of siliciclastic material over time in Lake Iseo deep basin. Therefore, results from our mixing model can be reliably used to discuss the evolution of the contribution of each source in terms of temporal variations in erosion processes in the catchment.

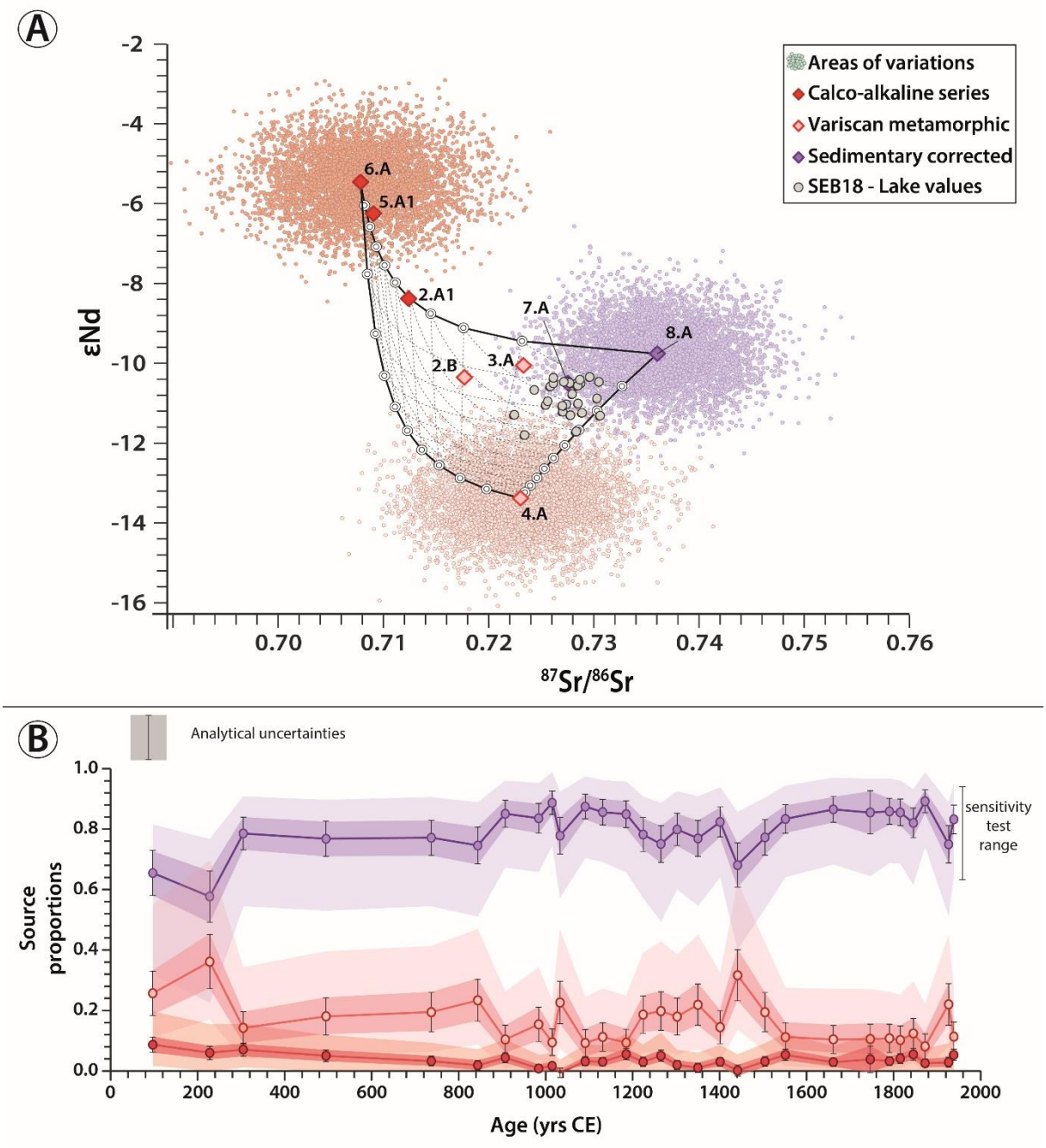

409

410 *Figure 5 – Results from the mixing model. (A) Nd-Sr isotope signatures of the three identified rock sources, used as end*
411 *members for explaining the composition of lake sediments. Samples 6.A, 8.A and 4.A are used to constrain the composition of*
412 *the rock end members. Lake sediments are shown as grey circles within an array described by mixing hyperbolae. The pink,*
413 *red, and purple symbols correspond to the composition of each Monte Carlo iteration used for the sensitivity test. (B) Fractional*
414 *contributions of each rock source to Lake Iseo sediment against time (yr CE). The propagation of analytical uncertainties are*
415 *represented as error bars and by dark shaded areas, corresponding to the D84 and D16 of the distribution of the parameters*
416 *obtained from Monte Carlo simulations. The light shaded areas represent the propagation of the uncertainty associated to*

the composition of the three rock sources, again with the D84 and D16 of the distribution of the parameters obtained from Monte Carlo simulations.

4.4. Evaluation of the sediment yield

Once the proportion of each sediment source to lake sediments has been calculated, river loads, and corresponding sediment yields can be estimated to obtain a quantitative assessment of catchment-scale erosion rates, for each area in the catchment. Sediment accumulated in a sinking basin, such as natural lakes, is partly composed of river silt-sized material and of authigenic deposits; sand-sized material such as river bedload being in general deposited along the sides of the river channel or in the delta (Hinderer et al., 2013). Few or none of the authigenic carbonates produced in Lake Iseo are preserved in the deep basin of the lake, as demonstrated in other deep peri-Alpine lakes (Ramisch et al., 1999), making this lake the ideal candidate to reconstruct the evolution of river suspended load through time, and thus of erosion rates in the contributing catchment. The time-dependent erosion flux from the catchment was determined as follows by using the calculation of a siliciclastic flux (SCF; $g.cm^{-2}.yr^{-1}$) from the lake sediment samples:

$$SCF = NCIR \times SR \times DBD \quad (6)$$

Here NCIR is the fraction of non-carbonate ignition residue of the lake sediments; SR is the sedimentation rate ($cm.yr^{-1}$) derived from the age-depth-model; and DBD is the dry bulk density of the samples ($g.cm^{-3}$). The DBD used in the SCF calculation was smoothed using a weighted arithmetic mean to reduce the impact of measurement bias in successive samples.

The sediment yield is defined as the mass of sediment that, over a given time span, leaves a boundary, such as the outlet of a catchment. SY is expressed in units of mass per unit of area and time (Hinderer et al., 2013 and reference therein). This parameter is used here to enable comparison with previous studies on erosion in the Alps. To calculate SY for the Iseo catchment, the total amount of sediment stored in Lake Iseo per amount of time ($Stock_{sed}$) needs to be estimated:

$$Stock_{sed} = SCF \times Lake\ area \quad (7)$$

SR may vary spatially over the surface of a lake. To calculate a consistent $Stock_{sed}$ for the entire lake we consider only the fraction of the total lake area where SR should be commensurate with that measured at the coring site. We assume here that this area corresponds to the flat part of the deep basin as suggested by the seismic survey (Bini et al., 2007), which lies below the slope discontinuity. Based on the lake bathymetry, we consider that the lake area with water depth below 210 m b.l.s should be taken into account in the calculation of $Stock_{sed}$, corresponding to a total of 18 km² (**supplementary S10**). The sediment stock is then multiplied by the contribution of each source to the lake sediment, in order to calculate changes in the source-specific sediment loads (SL, in t.yr^{-1}) through time:

$$SL = Stock_{sed} \times source\ proportion \quad (8)$$

To obtain an area-normalized sediment yield value for each source (SY_i), SL is normalized to the drainage area of each rock type. A value for total sediment yield (SY_{Total}) was also computed from the total SL:

$$SY_i = \frac{SL}{Source\ area} \quad (9)$$

$$SY_{Total} = \frac{SL}{Watershed\ area} \quad (10)$$

with SY_i and SY_{Total} expressed in t.km^{-2}.yr^{-1}. For the computation of SY_i and SY_{Total}, only the parts of the catchment area likely to be subjected to physical erosion are considered. For more detail on these calculations, see **supplementary S11**.

During the Industrial Age, $SY_{Sedimentary\ rocks}$ and $SY_{Calco\text{-}alkaline}$, representing area-specific erosion rates of the sedimentary and the calco-alkaline rocks areas in the Iseo catchment, show values around 100 and 10 t.km^{-2}.yr^{-1}, respectively (**Fig. 6**). $SY_{Sedimentary\ rocks}$ values for the recent times are coherent with estimates derived from the RUSLE model for similar contexts (Panagos et al., 2015; **supplementary S12**)**.** Calculated $SY_{Sedimentary\ rocks}$ values for the twentieth century are also close to present-day sediment yield measurements on Alpine rivers (30 – 671 t.km^{-2}.yr^{-1}; Hinderer et al., 2013). Deviations between

our calculations and previously reported values can be explained by storage of sediment in the lake delta (Hinderer et al., 2013) and by the absence of consideration of the bed load in our calculation. However, Hinderer et al. (2013) showed that in the southern crystalline Alps, where Lake Iseo is located, suspended load generally dominates over bed load. Altogether the present-day sediment yield estimated here for the Lake Iseo catchment is consistent with previously reported figures, lending support to our estimates of erosion rates through time.

5. Discussion

5.1. The record of erosion in Val Camonica

The calculated SY_{Total} is about 20 $t.km^{-2}.yr^{-1}$ during the Roman Period (**Fig. 6A**). From then on, SY_{Total} values increase nearly two-fold until the Medieval Period, when it reaches values between 30 and 40 $t.km^{-2}.yr^{-1}$. Then, SY_{Total} values decrease slightly until 1661 CE, prior to a sharp increase again during the Industrial Age and until the present.

Over centennial to millennial time scales, erosion is mainly a result of climate, vegetation, and land use changes (e.g. Bosco et al., 2008; Panagos et al., 2015), the last two parameters being associated with human activities. To disentangle the impact of climate and human practices on erosion in the Lake Iseo catchment, we investigate separately the reconstructed sediment yields of the "sedimentary rock" and calco-alkaline rocks areas. Indeed, no or very few human activities are reported in the high-altitude part of the catchment (e.g. Biagi and Starnini, 2015). Conversely, a great number of glaciers and rock glaciers are present in this area (Scotti et al., 2013), making erosion there highly sensitive to climate induced glacial fluctuations. In contrast, human activities are widely developed at low- to mid-altitude levels in the Val Camonica, meaning that human and climate have an unquestioned influence on erosion rates in the "sedimentary rock" area. No further investigation was conducted here on the sediment yields of the metamorphic area because of the lack of information about land use over time

in this area, which was in addition certainly affected by a combination of glacier fluctuations and human activities such as grazing and deforestation (**Fig. 6B**).

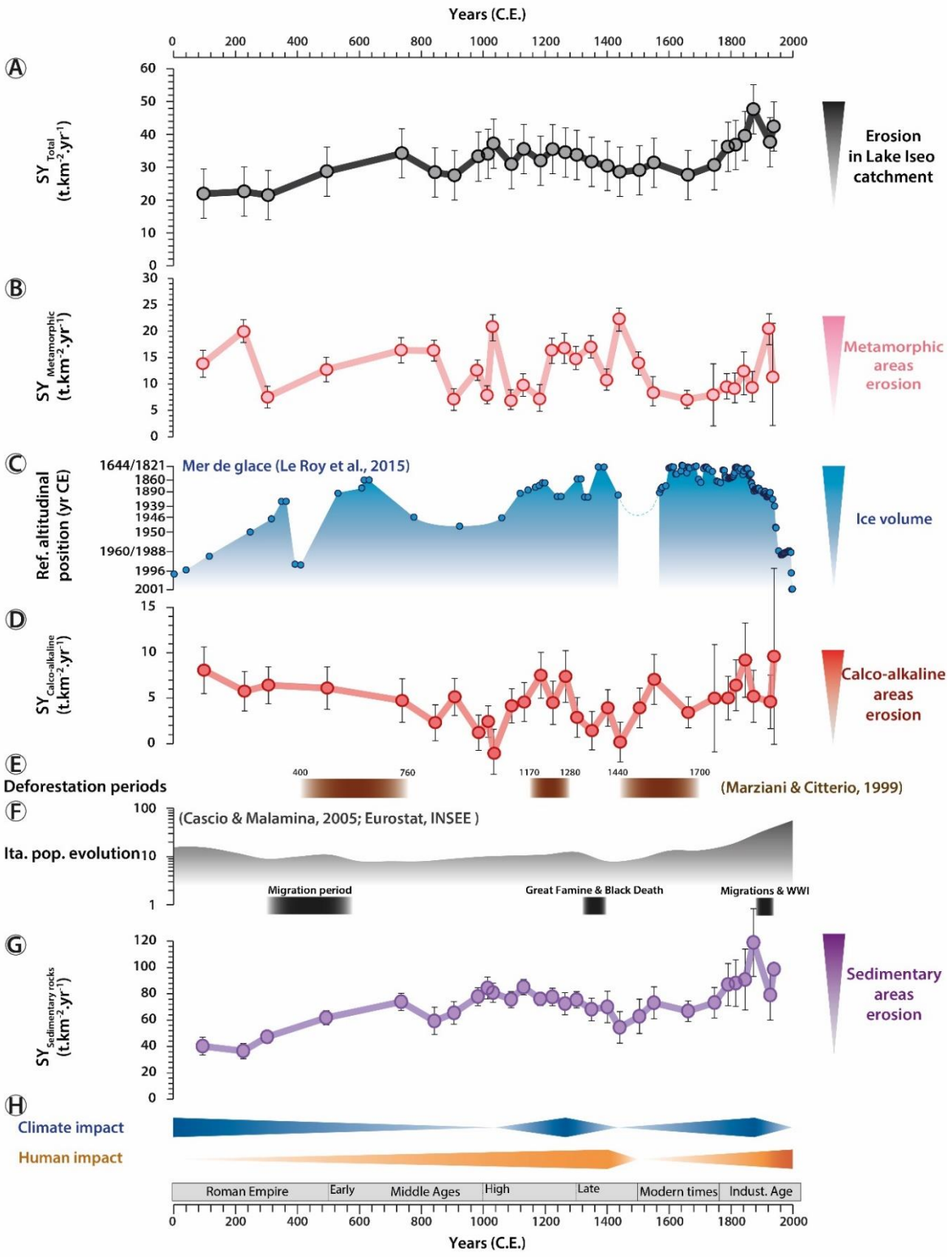

Figure 6 – Erosion in the Lake Iseo catchment and forcing factors evolution over the last 2000 years. From top to bottom: (A) total sediment yield obtained from the SEB18 sediment core (black curve); (B) the sediment yield originating from the erosion

of metamorphic areas in the Iseo catchment (pink curve); (C) the advances and retreats of the Mer de Glace glacier (French Alps, 45° 54.9'N and 6° 56.2'E) modified from Le Roy et al. (2015; blue shaded curve); (D) the sediment yield originating from the erosion of calco-alkaline rocks areas in the Iseo catchment (red curve); (E) the attested deforestation periods at a mid-altitude archaeological site of the Val Camonica valley (Marziani and Citterio, 1999; brown shades); (F) the evolution of the Italian population modified from Cascio and Malanima (2005) and Eurostat and INSEE sources (black shaded curve); demographic events that have affected the Italian population (black shades); (G) the sediment yield originating from the erosion of "sedimentary rock" area in the Iseo catchment (purple curve); (H) inferred periods of enhanced impact of climate (blue) and human (orange) activities on the erosion of the Iseo catchment.

5.1.1. Climate impact on erosion of high-altitude areas

Erosion in the high-altitude area of the Adamello massif is influenced by glacier advances and retreats and by extreme precipitation events. Glacier volumes depend on summer temperature and winter precipitation amounts (e.g. Fouinat et al., 2017; Holzhauser et al., 2005; Le Roy et al., 2015), all linked to Mediterranean climate. Therefore, in order to discuss the impact of climate fluctuations on erosion in Lake Iseo catchment, we focus on the $SY_{Calco\text{-}alkaline}$ reconstruction. Currently, glaciers present in the calco-alkaline rocks area of Lake Iseo catchment correspond to a small glacial tongue (0.7 km²) of the great Adamello glacier (21.6 km²) and small glacier bodies (< 0.5 km²) south and north of it. By their sizes, these glacier bodies are thought to be more sensitive to local climate change and present a lower inertia during glacier retreat than great Alpine glaciers.

$SY_{Calco\text{-}alkaline}$ first decreases from 100 to 1000 CE before increasing sharply until 1200 CE. The erosion from calco-alkaline rocks area remains high (> 6 $t.km^{-2}.yr^{-1}$) until 1300 CE before decreasing again until 1450 CE. Another increase is observed until 1550 CE. $SY_{Calco\text{-}alkaline}$ values remain high until the present days, with two peaks at 1845 CE and 1940 CE. The comparison of $SY_{Calco\text{-}alkaline}$ evolution over the last 2000 years with other alpine glaciers advances and retreats such as that of the Mont Blanc valley (**Fig. 6C**, Le Roy et al., 2015), or smaller glacial bodies (e.g. Fouinat et al., 2017; Glur et al., 2015) presents similarities. Except for the Roman Period, $SY_{Calco\text{-}alkaline}$ increases during periods of major glacier advances and decreases during retreat periods (**Fig. 7D**). During the Roman Period, $SY_{Calco\text{-}alkaline}$ present high values that are not consistent with the relatively low volume of great glaciers in the European

Alps (Holzhauser et al., 2005; Le Roy et al., 2015). However, erosion signals from small glacial bodies in the western French Alps (Fouinat et al., 2017) or in the Central Alps (Glur et al., 2015), present several peaks of enhanced erosion between 0 to 600 CE in relation to short term temperature variation, but the sampling resolution presented here do not allow the comparison.

From ~500 to 1000 CE, $SY_{Calco\text{-}alkaline}$ decreases in agreement with the volume of major great Alpine glaciers (Holzhauser et al., 2005; Le Roy et al., 2015). At that period, climate is warm and dry in the southern Alps, favouring glacier retreats (Büntgen et al., 2011). From 1000 to 1200 CE, erosion in high-altitude areas of Lake Iseo catchment increases sharply and remains high until 1300 CE. This period known as the High Medieval Advance (HMA) corresponds to a general episode of glacier advance in the Alps (Le Roy et al., 2015 and references therein) despite temperature increase in Europe (Büntgen et al., 2011). After the HMA, $SY_{Calco\text{-}alkaline}$ decreases again until 1450 CE before another increase, observable in every alpine glacier chronicle, and corresponding to the onset of the Little Ice Age (LIA; **Figs. 6C**). This period is characterized by a globally cold and wet climate, inducing significant glacier advances that caused intense erosion throughout the alpine area (e.g. Fouinat et al., 2017; Glur et al., 2015; Holzhauser et al., 2005; Le Roy et al., 2015). The LIA is known to last approximately until the middle of the nineteenth century, which correspond to the penultimate observed peak in $SY_{Calco\text{-}alkaline}$.

Collectively, these observations suggest, as demonstrated elsewhere in the Alps (e.g. Fouinat et al., 2017; Glur et al., 2015), that even over short time scales, colder periods induced higher erosion rates in the mountainous parts of the Lake Iseo catchment, implying a strong link between climate and erosion in high-altitude areas.

5.1.2. Human impact on erosion of low-altitude areas

At lower altitudes, climate fluctuations are not the only factors responsible for changes in erosion rates. Indeed, with land use and vegetation cover management, humans play a key role on erosion (e.g. Bosco et al., 2008; Panagos et al., 2015). However, during periods of high $SY_{Calco\text{-}alkaline}$, climatic

545 forcing of the erosion in the low-altitude such as the sedimentary area need to be considered together
546 with the human forcing as a possible driver of erosion.

547 The $SY_{Sedimentary\ rocks}$ values increase two-fold from the Roman Period until the High Middle Ages. This
548 increase occurs during dry and warm climate conditions across Europe (Bini et al., 2020; Büntgen et
549 al., 2011), and is associated with a gradual decrease of the $SY_{Calco\text{-}alkaline}$ signal (**Fig. 6D**), suggesting that
550 human practices become the main driver of erosion in the Lake Iseo catchment at that time.
551 Abandonment of forest management plans until the Migration Period (300 – 570 CE) has been
552 attributed to a declining influence of the Roman Empire in the Lake Iseo catchment (Comiti, 2012). The
553 period from the Roman Period until the High Middle Ages is interpreted as a period of enhanced human
554 pressure on the environment due to:

555 (i) Deforestation to allow for instance for increased mining activity, as observable elsewhere
556 in Europe (Büntgen et al., 2011) and at low- to mid-altitude sites in the Val Camonica (**Fig.**
557 **6E**, Marziani and Citterio, 1999; Pini, 2002; Pini et al., 2016);
558 (ii) A general population increase in Italy towards the Middle Ages (**Fig. 6F**, Cascio and
559 Malanima, 2005);
560 (iii) An intensification of land use and human practices, coupled with replacement of pre-
561 existent buildings (Büntgen et al., 2011).

562 In the Iseo catchment, the collapse of the forest management system of the Roman Empire should be
563 at the origin of an enhancement of erosion. During the High Middle Ages and until the Late Middle
564 Ages, $SY_{Sedimentary\ rocks}$ remains relatively high (**Fig. 6G**). At that time, regional climate is wet (Bini et al.,
565 2020; Büntgen et al., 2011), extreme precipitations are frequent locally until 1300 CE (Wirth et al.,
566 2013), and the human pressure remains important, with (i) attested periods of deforestation in the
567 catchment (Marziani and Citterio, 1999) and (ii) intense land use and pastoralism in the Italian Alps
568 (Büntgen et al., 2011; Comiti, 2012; Joannin et al., 2014; Pini, 2002). Therefore, disentangling human
569 and climate forcing over this period is not possible, and it is likely that the combination of the two

570 factors induced intense erosion in the entire Lake Iseo catchment until the Great Famine (1315 – 1317
571 CE) and the Black Death (1347 – 1351 CE). A slight decrease in $SY_{Sedimentary\ rocks}$ is observed just after
572 these two (**Fig. 7G, F**). These events are known to have deeply impacted European populations,
573 resulting in particular in agricultural decline in the Southern Alps (e.g. Büntgen et al., 2011; Joannin et
574 al., 2014; Ruddiman, 2007).

575 After this trough, $SY_{Sedimentary\ rocks}$ increases progressively until 1800 CE and then strongly until 1872 CE
576 and the onset of the Industrial Age (**Fig. 6G**). Two hypotheses can be invoked to explain this pattern:
577 the effect of the Little Ice Age (LIA) following an increase of human activity. Indeed, maximal glacier
578 advances in the Alps are reported at around 1850 CE (Holzhauser et al., 2005; Le Roy et al., 2015),
579 before the current period of general retreat. The LIA is also characterized by more frequent extreme
580 precipitation events in the Southern Alps (Wirth et al., 2013). The effect of LIA climate change on
581 erosion, through precipitation events and plausible glacier advances, are well visible on $SY_{Calco\text{-}alkaline}$ at
582 that time and thus cannot be ignored for the interpretation of the low and mid-altitude part erosion
583 signal of the Lake Iseo catchment, even if the LIA starts before the increase in $SY_{Calco\text{-}alkaline}$.
584 Synchronously, human pressure on the environment grows sharply in the Italian Alps generally, and in
585 the Lake Iseo catchment in particular, with an increase of the population (Cascio and Malanima, 2005)
586 associated to a surge in agricultural practices and a transition towards intensive farming (Federico and
587 Malanima, 2004).

588 Between 1872 and 1926 CE, $SY_{Sedimentary\ rocks}$ decreases sharply, most likely due to the onset of outward
589 migration, with more than 11 million people leaving Italy for the New World (Moretti, 1999). $SY_{Sedimentary\ rocks}$
590 finally increases until 1938 CE (last sample).

591 To summarize, each episode of $SY_{Sedimentary\ rocks}$ increase in the Lake Iseo catchment can be associated
592 to a period of intense human pressure on the environment (**Fig. 6**). Between 1030 and 1300 CE and
593 during the LIA, wetter and colder climate favoured erosion not only at high altitudes but also at
594 intermediate and low altitudes, making it hard to disentangle climate versus human influences.

However, from the Roman Period to the Middle Ages and up to the present, erosion at low altitudes shows a clear increase, asynchronous and decorrelated from the regional climate trend. Therefore, only human pressure on the environment can be responsible for this trend (**Fig. 6H**). Human activities, through the development of agricultural practices and deforestation at low- and mid-altitude have induced a three-fold increase in erosion rates in a large catchment of the Italian Alps. Hence, even in large mountainous catchments, human activities affect the CZ by increasing erosion, resulting in damages on ecosystems and in soil and biomass carbon shrinkage. The CZ is deteriorated by human practices for 2000 years in the Alps, making it highly sensitive to the current anthropization pressure. Long term erosion chronicles, such as those produced from lake sediments, are critical to quantify the influence of the different forcing factors impacting CZ erosion through time.

6. Conclusion

Contributions of glacial variability and human activities to erosion were reconstructed from a sediment core with a stable isotope mixing model. The absolute value of sediment yields signal is highly coherent with previous work and annual average erosion models, making it possible to interpret its variations reported in the three mains sources. The erosion signal from high-altitude areas, synchronous with the three main episodes of European glacier advances and retreats, is interpreted to be driven by climatic fluctuations. From the comparison between the erosion signals of high- and low-altitude areas, we were able to disentangle the main triggers of the erosion at low-altitude areas in the study area. Human activities, through deforestation, agricultural practices and grazing become the main forcing factors affecting erosion between the Roman Period and the Middle Ages, and from the Late Middle Ages to the present. A three-fold increase, from 36 to 118 $t.km^{-2}.yr^{-1}$ is observed in anthropized areas. This is the first time that the impact of human activity on catchment-scale erosion is quantitatively assessed over time, based on lake sediments. These findings should contribute to enhance modelling of human impacts on Critical Zone erosion and on carbon shrinkage in soils.

Acknowledgments

This work was financed by CRITLAKE project co-funded by EC2CO and AAP Université Savoie Mont Blanc. Parts of this work were also supported by IPGP multidisciplinary programme PARI and by Paris-IdF region SESAME Grant No. 12015903. We wish to thank the support of the entire staff of the C2FN-DT-INSU associated to the CLIMCORE project. ^{14}C analyses were acquired thanks to the CNRS-INSU ARTEMIS national radiocarbon AMS measurement programme at Laboratoire de Mesure ^{14}C (LMC14) in the CEA Institute at Saclay (French Atomic Energy Commission).

We are grateful to Pierre Burckel for help with Q-ICP-MS measurements; to Laëticia Faure for her valuable help and assistance with lab work; to Pascale Louvat, Thibaud Sondag, and Barthélémy Julien for assistance with MC-ICP-MS measurements; and to Ana Brancelj for the help on the field during river samples collection. We wish to thank Damien Guinoiseau for helpful conversations about the interpretation of isotope data. The authors are grateful to the editors P. Rioual and G. Zanchetta for their comments and help during the review processing and to the two anonymous reviewers.

References

Angima, S.D., Stott, D.E., O'neill, M.K., Ong, C.K., Weesies, G.A., 2003. Soil erosion prediction using RUSLE for central Kenyan highland conditions. Agric. Ecosyst. Environ. 97, 295–308.

Appleby, P.G., Richardson, N., Nolan, P.J., 1991a. 241Am dating of lake sediments, in: Smith, J.P., Appleby, P.G., Battarbee, R.W., Dearing, J.A., Flower, R., Haworth, E.Y., Oldfield, F., O'Sullivan, P.E. (Eds.), Environmental History and Palaeolimnology, Developments in Hydrobiology. Springer Netherlands, pp. 35–42.

Appleby, P.G., Richardson, N., Nolan, P.J., 1991b. 241Am dating of lake sediments, in: Smith, J.P., Appleby, P.G., Battarbee, R.W., Dearing, J.A., Flower, R., Haworth, E.Y., Oldfield, F., O'Sullivan, P.E. (Eds.), Environmental History and Palaeolimnology, Developments in Hydrobiology. Springer Netherlands, pp. 35–42. https://doi.org/10.1007/978-94-011-3592-4_4

Arnaud, F., Poulenard, J., Giguet-Covex, C., Wilhelm, B., Révillon, S., Jenny, J.-P., Revel, M., Enters, D., Bajard, M., Fouinat, L., others, 2016. Erosion under climate and human pressures: An alpine lake sediment perspective. Quat. Sci. Rev. 152, pp. 1-18. https://doi.org/10.1016/j.quascirev.2016.09.018

Bajard, M., Poulenard, J., Sabatier, P., Bertrand, Y., Crouzet, C., Ficetola, G.F., Blanchet, C., Messager, E., Giguet-Covex, C., Gielly, L., Rioux, D., Chen, W., Malet, E., Develle, A.-L., Arnaud, F., 2020. Pastoralism increased vulnerability of a subalpine catchment to flood hazard through changing soil properties. Palaeogeogr. Palaeoclimatol. Palaeoecol. 538, 109462. https://doi.org/10.1016/j.palaeo.2019.109462

Bajard, M., Sabatier, P., David, F., Develle, A.-L., Reyss, J.-L., Fanget, B., Malet, E., Arnaud, D., Augustin, L., Crouzet, C., Poulenard, J., Arnaud, F., 2016. Erosion record in Lake La Thuile sediments (Prealps, France): Evidence of montane landscape dynamics throughout the Holocene. The Holocene 26, 350–364. https://doi.org/10.1177/0959683615609750

Biagi, P., Starnini, E., 2015. Human settlement and environmental exploitation of Valcamonica-Valtrompia watershed from the beginning of the Holocene to the Middle Ages. Nat. Brescia. 39, 195.

Bini, A., Corbari, D., Falletti, P., Fassina, M., Perotti, C.R., Piccin, A., 2007. Morphology and geological setting of Iseo Lake (Lombardy) through multibeam bathymetry and high-resolution seismic profiles. Swiss J. Geosci. 100, 23–40.

Bini, A., Forcella, F., Corbari, D., Facchinetti, P., Ferliga, C., Pisani, V., Rigamonti, I., Rossi, S., Zanotti, M., Berra, F., 2012. Foglio 078 Breno. Carta Geologica d'Italia alla scala 1: 50.000.

Bini, M., Zanchetta, G., Regattieri, E., Isola, I., Drysdale, R.N., Fabiani, F., Genovesi, S., Hellstrom, J.C., 2020. Hydrological changes during the Roman Climatic Optimum in northern Tuscany (Central Italy) as evidenced by speleothem records and archaeological data. J. Quat. Sci. 35, 791–802. https://doi.org/10.1002/jqs.3224

Blaauw, M., 2010. Methods and code for 'classical'age-modelling of radiocarbon sequences. Quat. Geochronol. 5, 512–518.

Blaauw, M., Christen, J.A., Lopez, M.A.A., Vazquez, J.E., V, O.M.G., Belding, T., Theiler, J., Gough, B., Karney, C., 2021. rbacon: Age-Depth Modelling using Bayesian Statistics.

Borrelli, P., Robinson, D.A., Panagos, P., Lugato, E., Yang, J.E., Alewell, C., Wuepper, D., Montanarella, L., Ballabio, C., 2020. Land use and climate change impacts on global soil erosion by water (2015-2070). Proc. Natl. Acad. Sci. 117, 21994–22001.

Bosco, C., Rusco, E., Montanarella, L., Oliveri, S., 2008. Soil erosion risk assessment in the alpine area according to the IPCC scenarios. Threats Soil Qual. Eur. Ed. Toth G Montanarella Rusco E EUR 23438, 47–58. http://www.nat-hazards-earth-syst-sci.net/15/225/2015/

Brack, P., Dal Piaz, G.V., Baroni, C., Carton, A., Nardin, M., Pellegrini, G.B., Pennacchioni, G., 2008. Note illustrative della Carta Geologica d'Italia alla scala 1: 50.000. Foglio 058, Monte Adamello. Carta Geol. Ital. Alla Scala 1 50000.

Brazier, J.-M., Schmitt, A.-D., Pelt, E., Lemarchand, D., Gangloff, S., Tacail, T., Balter, V., 2020. Determination of Radiogenic 87Sr/86Sr and Stable δ88/86SrSRM987 Isotope Values of Thirteen Mineral, Vegetal and Animal Reference Materials by DS-TIMS. Geostand. Geoanalytical Res. 44, 331–348. https://doi.org/10.1111/ggr.12308

Bruel, R., Sabatier, P., 2020. serac: an R package for ShortlivEd RAdionuclide chronology of recent sediment cores. J. Environ. Radioact. 225, 106449. https://doi.org/10.1016/j.jenvrad.2020.106449

Büntgen, U., Tegel, W., Nicolussi, K., McCormick, M., Frank, D., Trouet, V., Kaplan, J.O., Herzig, F., Heussner, K.-U., Wanner, H., Luterbacher, J., Esper, J., 2011. 2500 Years of European Climate Variability and Human Susceptibility. Science 331, 578–582. https://doi.org/10.1126/science.1197175

Caro, G., Bourdon, B., Birck, J.-L., Moorbath, S., 2006. High-precision 142Nd/144Nd measurements in terrestrial rocks: Constraints on the early differentiation of the Earth's mantle. Geochim. Cosmochim. Acta 70, 164–191. https://doi.org/10.1016/j.gca.2005.08.015

Cascio, E.L., Malanima, P., 2005. Cycles and Stability. Italian Population before the Demographic Transition (225 B.C. - A.D. 1900). Riv. Storia Econ. https://doi.org/10.1410/20933

Chiesa, S., Micheli, P., Cariboni, M., Tognini, P., Motta, L., Longhin, M., Zambrotti, P., Marcato, E., Ferrario, A., 2011. Note illustrative della Carta Geologica d'Italia alla scala 1: 50.000, Foglio 41 Ponte di Legno. CARG ISPRA Ist. Super. Prot. E Ric. Ambient. Roma P 169.

Cogez, A., Meynadier, L., Allègre, C., Limmois, D., Herman, F., Gaillardet, J., 2015. Constraints on the role of tectonic and climate on erosion revealed by two time series analysis of marine cores around New Zealand. Earth Planet. Sci. Lett. 410, 174–185. https://doi.org/10.1016/j.epsl.2014.11.029

Collins, A.L., Walling, D.E., 2002. Selecting fingerprint properties for discriminating potential suspended sediment sources in river basins. J. Hydrol. 261, 218–244. https://doi.org/10.1016/S0022-1694(02)00011-2

Comiti, F., 2012. How natural are Alpine mountain rivers? Evidence from the Italian Alps. Earth Surf. Process. Landf. 37, 693–707. https://doi.org/10.1002/esp.2267

Croke, J., 2004. HYDROLOGY | Soil Erosion Control, in: Burley, J. (Ed.), Encyclopedia of Forest Sciences. Elsevier, Oxford, pp. 387–397. https://doi.org/10.1016/B0-12-145160-7/00270-2

FAO, I., 2015. Status of the world's soil resources (SWSR)–main report. Food Agric. Organ. U. N. Intergov. Tech. Panel Soils Rome Italy 650.

Faure, G., Assereto, R., Tremba, E.L., 1978. Strontium isotope composition of marine carbonates of Middle Triassic to Early Jurassic age, Lombardic Alps, Italy*. Sedimentology 25, 523–543. https://doi.org/10.1111/j.1365-3091.1978.tb02078.x

Federico, G., Malanima, P., 2004. Progress, decline, growth: product and productivity in Italian agriculture, 1000–2000. Econ. Hist. Rev. 57, 437–464. https://doi.org/10.1111/j.1468-0289.2004.00284.x

Fouinat, L., Sabatier, P., Poulenard, J., Etienne, D., Crouzet, C., Develle, A.-L., Doyen, E., Malet, E., Reyss, J.-L., Sagot, C., Bonet, R., Arnaud, F., 2017. One thousand seven hundred years of interaction between glacial activity and flood frequency in proglacial Lake Muzelle (western French Alps). Quat. Res. 87, 407–422. https://doi.org/10.1017/qua.2017.18

Garibaldi, L., Mezzanotte, V., Brizzio, M.C., Rogora, M., Mosello, R., 1999. The trophic evolution of Lake Iseo as related to its holomixis. J. Limnol. 58, 10. https://doi.org/10.4081/jlimnol.1999.10

Gayer, E., Michon, L., Louvat, P., Gaillardet, J., 2019. Storm-induced precipitation variability control of long-term erosion. Earth Planet. Sci. Lett. 517, 61–70. https://doi.org/10.1016/j.epsl.2019.04.003

Glur, L., Stalder, N.F., Wirth, S.B., Gilli, A., Anselmetti, F.S., 2015. Alpine lacustrine varved record reveals summer temperature as main control of glacier fluctuations over the past 2250 years. The Holocene 25, 280–287. https://doi.org/10.1177/0959683614557572

Gosso, G., Spalla, M., G.B, S., Berra, F., Bini, A., F, F., 2012. Note illustrative della Carta Geologica d'Italia alla scala 1:50.000. Foglio 057 - Malonno, I.S.P.R.A.

Hajj, F., Poszwa, A., Bouchez, J., Guérold, F., 2017. Radiogenic and "stable" strontium isotopes in provenance studies: A review and first results on archaeological wood from shipwrecks. J. Archaeol. Sci. 86, 24–49. https://doi.org/10.1016/j.jas.2017.09.005

Heiri, O., Lotter, A.F., Lemcke, G., 2001. Loss on ignition as a method for estimating organic and carbonate content in sediments: reproducibility and comparability of results. J. Paleolimnol. 25, 101–110.

Hinderer, M., Kastowski, M., Kamelger, A., Bartolini, C., Schlunegger, F., 2013. River loads and modern denudation of the Alps — A review. Earth-Sci. Rev. 118, 11–44. https://doi.org/10.1016/j.earscirev.2013.01.001

Holzhauser, H., Magny, M., Zumbuühl, H.J., 2005. Glacier and lake-level variations in west-central Europe over the last 3500 years. The Holocene 15, 789–801. https://doi.org/10.1191/0959683605hl853ra

Jacobsen, S.B., Wasserburg, G.J., 1980. Sm-Nd isotopic evolution of chondrites. Earth Planet. Sci. Lett. 50, 139–155. https://doi.org/10.1016/0012-821X(80)90125-9

Joannin, S., Magny, M., Peyron, O., Vannière, B., Galop, D., 2014. Climate and land-use change during the late Holocene at Lake Ledro (southern Alps, Italy). The Holocene 24, 591–602.

Kagami, H., Ulmer, P., Hansmann, W., Dietrich, V., Steiger, R.H., 1991. Nd-Sr isotopic and geochemical characteristics of the southern Adamello (northern Italy) intrusives: Implications for crustal versus mantle origin. J. Geophys. Res. Solid Earth 96, 14331–14346.

Le Roy, M., Nicolussi, K., Deline, P., Astrade, L., Edouard, J.-L., Miramont, C., Arnaud, F., 2015. Calendar-dated glacier variations in the western European Alps during the Neoglacial: the

Mer de Glace record, Mont Blanc massif. Quat. Sci. Rev. 108, 1–22. https://doi.org/10.1016/j.quascirev.2014.10.033
Marziani, G., Citterio, S., 1999. The effects of human impact on the arboreal vegetation near ancient iron smelting sites in Val Gabbia, northern Italy. Veg. Hist. Archaeobotany 8, 225–229. https://doi.org/10.1007/BF02342722
Millward, A.A., Mersey, J.E., 1999. Adapting the RUSLE to model soil erosion potential in a mountainous tropical watershed. Catena 38, 109–129.
Mittempergher, S., Zanchi, A., Zanchetta, S., Fumagalli, M., Gukov, K., Bistacchi, A., 2021. Fault reactivation and propagation in the northern Adamello pluton: The structure and kinematics of a kilometre-scale seismogenic source. Tectonophysics 806, 228790. https://doi.org/10.1016/j.tecto.2021.228790
Montgomery, D., 2012. Dirt – The Erosion of Civilizations, 2nd edition. ed. University of California Press, Berkeley.
Moretti, E., 1999. Social Networks and Migrations: Italy 1876–1913. Int. Migr. Rev. 33, 640–657. https://doi.org/10.1177/019791839903300304
Panagos, P., Borrelli, P., Poesen, J., Ballabio, C., Lugato, E., Meusburger, K., Montanarella, L., Alewell, C., 2015. The new assessment of soil loss by water erosion in Europe. Environ. Sci. Policy 54, 438–447. https://doi.org/10.1016/j.envsci.2015.08.012
Pilotti, M., Valerio, G., Leoni, B., 2013. Data set for hydrodynamic lake model calibration: A deep prealpine case. Water Resour. Res. 49, 7159–7163.
Pini, R., 2002. A high-resolution Late-Glacial – Holocene pollen diagram from Pian di Gembro (Central Alps, Northern Italy). Veg. Hist. Archaeobotany 11, 251–262. https://doi.org/10.1007/s003340200038
Pini, R., Ravazzi, C., Aceti, A., Castellano, L., Perego, R., Quirino, T., Valle', F., 2016. Ecological changes and human interaction in Valcamonica, the rock art valley, since the last deglaciation 29, 19–34.
Ramisch, F., Dittrich, M., Mattenberger, C., Wehrli, B., Wüest, A., 1999. Calcite dissolution in two deep eutrophic lakes. Geochim. Cosmochim. Acta 63, 3349–3356. https://doi.org/10.1016/S0016-7037(99)00256-2
Reimer, P.J., Austin, W.E.N., Bard, E., Bayliss, A., Blackwell, P.G., Bronk Ramsey, C., Butzin, M., Cheng, H., Edwards, R.L., Friedrich, M., Grootes, P.M., Guilderson, T.P., Hajdas, I., Heaton, T.J., Hogg, A.G., Hughen, K.A., Kromer, B., Manning, S.W., Muscheler, R., Palmer, J.G., Pearson, C., van der Plicht, J., Reimer, R.W., Richards, D.A., Scott, E.M., Southon, J.R., Turney, C.S.M., Wacker, L., Adolphi, F., Büntgen, U., Capano, M., Fahrni, S.M., Fogtmann-Schulz, A., Friedrich, R., Köhler, P., Kudsk, S., Miyake, F., Olsen, J., Reinig, F., Sakamoto, M., Sookdeo, A., Talamo, S., 2020. The IntCal20 Northern Hemisphere Radiocarbon Age Calibration Curve (0–55 cal kBP). Radiocarbon 62, 725–757. https://doi.org/10.1017/RDC.2020.41
Renard, K.G., Foster, G.R., Weesies, G.A., Porter, J.P., 1991. RUSLE: Revised universal soil loss equation. J. Soil Water Conserv. 46, 30–33.
Reyss, J.-L., Schmidt, S., Legeleux, F., Bonté, P., 1995. Large, low background well-type detectors for measurements of environmental radioactivity. Nucl. Instrum. Methods Phys. Res. Sect. Accel. Spectrometers Detect. Assoc. Equip. 357, 391–397.
Ruddiman, W.F., 2007. The early anthropogenic hypothesis: Challenges and responses. Rev. Geophys. 45. https://doi.org/10.1029/2006RG000207
Rusco, E., Montanarella, L., Bosco, C., 2008. Soil Erosion: a main threats to the soil in Europe. pp. 37–46.
Scotti, R., Brardinoni, F., Alberti, S., Frattini, P., Crosta, G.B., 2013. A regional inventory of rock glaciers and protalus ramparts in the central Italian Alps. Geomorphology 186, 136–149. https://doi.org/10.1016/j.geomorph.2012.12.028
Wirth, S.B., Gilli, A., Simonneau, A., Ariztegui, D., Vannière, B., Glur, L., Chapron, E., Magny, M., Anselmetti, F.S., 2013. A 2000 year long seasonal record of floods in the southern European Alps. Geophys. Res. Lett. 40, 4025–4029. https://doi.org/10.1002/grl.50741